The Effects of Orientation and Crystallinity on the Solvent-Induced Crystallization of Poly(ethylene Terephthalate). II. Physical Structure and Morphology

HASAN JAMEEL, HERMAN D. NOETHER, and LUDWIG REBENFELD, *Textile Research Institute, and Department of Chemical Engineering, Princeton University, Princeton, New Jersey*

Synopsis

This series of papers summarizes the results of an experimental research program designed to establish the effects of preexisting orientation and crystallinity on the solvent-induced crystallization of poly(ethylene terephthalate) films. Dimethylformamide was used as a model for a strongly interacting solvent. This paper deals with the morphological and structural modifications induced by the solvent crystallization process. The effects on the structure and morphology of the solvent crystallization were dominated by surface cavitation, creation of voids, and by changes in the degree of crystallinity. The surface structure varied from a spherulitic cavitated structure for films of low orientations (low draw ratios) to a smooth surface at the higher draw ratios. In addition to the change in the surface morphology, an internal void structure was formed due to crystallization taking place in a swollen state. The formation of voids is dependent on the treatment temperature, draw ratio, and the method of solvent removal. The voids collapse upon annealing at high temperatures. Increases in the degree of crystallinity and changes in orientation were dependent on the treatment temperature. The crystallite size goes through a maximum at an intermediate degree of orientation. The crystalline orientation decreases with increasing treatment temperature. The structures formed during solvent treatments did not show any characteristic premelting endotherms at the low draw ratios. In the case of higher draw ratios, a small premelting endotherm was noticeable at a temperature 70°C greater than that of the solvent treatment.

INTRODUCTION

It is generally recognized that in the presence of certain interactive liquids (solvents), crystallization of amorphous polymers can take place at temperatures well below the glass transition temperature (T_g) of the dry polymer. Indeed, solvent-induced crystallization (SINC) has been the subject of increasing interest for both amorphous and semicrystalline polymers. One reason for this interest is the recognition that the physical structure and morphology of SINC polymers may be significantly different from that produced by thermal and stress induced crystallization. The purpose of the work described in this series of papers is to examine the influence of preexisting orientation and crystallinity on the SINC process. The system studied was poly(ethylene terephthalate) (PET) films using dimethyl formamide (DMF) as a model strongly interacting crystallizing solvent. Paper I dealt with solvent sorption and diffusion related phenomena.[1] This paper examines the crystalline structure and the morphology of the films after the SINC process.

Journal of Applied Polymer Science, Vol. 27, 773–793 (1982)
 CCC 0021-8995/82/030773-21$02.10

BACKGROUND

Crystalline Structure

Early studies were somewhat controversial with regard to the morphology induced in unoriented amorphous polymers by the SINC process with evidence for both spherulitic and lamellar crystallization.[2,3] However, Desai and Wilkes[4] and also Makarewicz and Wilkes,[5] using both light scattering and scanning electron microscopy, have shown definitively that a spherulitic structure is the characteristic morphology resulting from SINC.

Except for the work of Weigmann and co-workers,[6–14] who studied the solvent-induced structural modifications in PET fibers, most of the earlier work on morphology had been limited to unoriented films. In fibers there was no evident spherulitic superstructure, and only discrete scattering was observed in small angle x-ray diffraction patterns.[12] Makarewicz and Wilkes[5] and Zachmann[15,16] have shown that unoriented PET solvent crystallized at 25°C does not exhibit sharp reflections in wide angle x-ray diffraction patterns, and the breadth corresponds approximately to PET that has been thermally crystallized at 90–100°C.

Much of the attention on the structural changes induced by SINC has been focused on the crystalline region, although Zachmann and co-workers[17,18] studied the amorphous domains using NMR-spectra. The narrow component of the spectrum of an acetone-crystallized PET sample showed small line broadening, implying the presence of swelling agents and suggesting that the polymer chains within the noncrystalline regions are under lower stress. In thermally crystallized PET the amorphous chains are usually under greater stress at equivalent levels of crystallinity.

Cavitation and Void Structure

In addition to the changes in the crystalline structure, SINC has been shown to cause extensive surface cavitation in some solvent systems. Cavitation is believed to be related to the degree of interaction that exists between the solvent and the polymer, with the more interactive solvents causing a greater extent of cavitation. The degree of surface cavitation also increases with increasing treatment temperatures.[4,5] Surface cavitation was not observed in the case of oriented PET fibers.

Some workers[2,19,20,21] have also presented evidence for internal cavitation which occurs at the center of the film when the two diffusion and crystallization fronts meet. However, internal fracture has not been observed in all cases. Makarewicz and Wilkes[5] reported the development of internal cavitation with some PET—solvent systems, while with PET—methylene chloride and PET—dioxane systems only a cavitated surface layer was observed. A cavitated boundary moving along with the diffusion front has also been reported.[4,5] A cylindrical void was observed at the center of low-denier, amorphous, unoriented (as spun) fibers after treatment in methylene chloride.[22] In the case of oriented fibers, internal fracture has not been observed after treatment with various solvents.[6–14] In addition to the surface and internal cavitation discussed above, there exists a distribution of voids and microvoids throughout the polymer matrix. For example, oriented PET yarns treated in DMF at 140°C followed by

a 100°C water rinse show an intense small angle x-ray scattering probably due to voids or microvoids within the fiber. The high intensity of the void scattering masks the discrete scattering which results from the lamellar structure. Weigmann and co-workers[11–14] have postulated that these voids result from crystallization taking place in the swollen state. Indeed, the void structure is one of the major differences between solvent and thermally crystallized PET, and in the case of fibers, is of particular importance in connection with dyeing behavior.

Melting Behavior

Melting behavior can also be utilized to characterize structure. Differential scanning calorimetry (DSC) melting curves are quite sensitive to changes that result from various crystallization processes. The occurrence of a double melting peak in DSC curves of PET has been quite well documented.[23–26] Amorphous PET can be crystallized upon treating the sample at a temperature above the glass transition (annealing). The structural changes brought about by the above treatment result in a structure which frequently exhibits two endothermic fusion peaks. The first peak is only noticeable when the PET has been annealed above a certain temperature for a sufficient length of time, and its position is determined by the annealing temperature. The second peak, usually much larger, is visible at a constant temperature.

Many views have been expressed as to the origin of the peaks. Bell and Murayama[27] theorized that the first peak is associated with crystals containing partially extended chains while the second peak results from a chain folded structure. Roberts,[28] on the other hand, interpreted the first peak as being due to chain-folded crystals and the second peak to bundlelike crystals. Most of the work since then shows that the multiple peaks are due to imperfections within the crystallites, and not due to different forms of crystals. Weigmann et al.[13,14] noted the presence of multiple melting peaks in heat set and solvent treated PET fibers.

Effect of Orientation

Very little work has been reported on the morphological changes brought about in polymers by SINC where there is a systematic variation of the initial structure. Sheldon[29] found that very low levels of orientation did not have any noticeable effect on either the kinetics or the morphology of benzene-treated polymers. Desai and Wilkes[4] and Makarewicz and Wilkes[5] observed that cold drawn samples do not exhibit noticeable surface cavitation when treated with highly interactive solvents at room temperature, even though the same solvents are capable of inducing extensive surface cavitation in unoriented, amorphous PET films. For oriented films, no change in the superstructures was observed after treatments in dioxane at 26°C, while after treatments in dioxane at 75°C a spherulitic pattern was present, especially when the sample was unrestrained.[30] This agrees with the observations made by Weigmann and co-workers[11] that no significant changes in properties are noticeable in drawn PET fibers below a treatment temperature of 100°C.

EXPERIMENTAL

Materials

The PET films used in these studies were obtained through the courtesy of G. C. Adams of E. I. du Pont de Nemours & Co., Inc.[31] Unoriented films of PET were drawn using two sets of rollers rotating at different speeds which determined the draw ratio. Two heaters were placed in between the sets of rollers, one on top of the film and one below. The heater settings determined the stretch temperature. An input power at 30% of rated heater power was used by du Pont, corresponding to a stretch temperature of 90–110°C. A range of draw ratios between 1.0 and 4.0 were provided.

Treatments

Film specimens were treated in reagent grade DMF by direct immersion in DMF maintained at a specified temperature. The time of immersion was selected so as to have complete solvent penetration as determined from weight uptake behavior at various temperatures. In the case of treatments at 21°C, the treatment time was 1 h for all the draw ratios, although complete penetration had not been achieved for the higher draw ratios. Unless otherwise indicated, the DMF treatments were performed in the unrestrained state, and were followed by an aftertreatment in water at 100°C for 5 min to facilitate DMF removal. The samples were subsequently vacuum dried over Drierite® for 1 day.

Scanning Electron Microscopy

The SEM studies to characterize the surface morphology were performed using an ISI Super-Mini SEM. The samples were observed using an accelerating voltage in the order of 15 kV. The samples were coated with a thin uniform layer of gold-palladium (100–200 Å), which allows one to study the surface morphology without causing any degradation of the polymer material due to the incidence of the high energy electron beam. It also gives an electron-rich surface which allows for better image quality and prevents charging. Cross sections of selected samples were also studied by SEM after fracturing the polymer sample cryogenically (brittle fracture) after immersion in liquid N_2.

Wide Angle X-ray Scattering

The wide angle x-ray scattering (WAXS) was carried out on a Philips x-ray-diffraction unit with an Ni filtered Cu K_α radiation source at 35 kW and 15 mA. Two pinhole collimators were used and the photographs were taken with a Statton vacuum camera using Ilford Industrial G x-ray film. The scattering patterns were scanned in both equatorial and meridional directions with a Joyce–Loebl microdensitometer.

Small Angle X-ray Scattering

Small angle x-ray scattering (SAXS) patterns were taken on a Philips XRG-3000 at 35 kV and 15 mA with a copper K_α line at 1.54 Å. Pinhole collimation was used with a nickel filter. The number of PET films and layers used to generate the pattern was such that the combined thickness was about the same in each case, 14–16 mils. The exposure time was determined by the amount of radiation required to photograph the characteristic pattern on film. The specimen was mounted on a flat plate at right angles to the incident x-ray beam. The beamstop was a precisely aligned lead piece on a wire and placed a few inches in front of the photographic plate. The sample to film distance was 250 mm, and the sample was placed outside the vacuum chamber. The pattern was recorded on Ilford Industrial G film and scanned on a Joyce–Loebl microdensitometer.

Differential Scanning Calorimetry

Calorimetric measurements were made on a du Pont DSC cell module connected to a 2990 Thermal Analyzer. The samples were about 5–10 mg, and the analyses were carried out in a nitrogen atmosphere. The heating rate was 10°C/min. The curves were recorded using two different sensitivities in order to detect both small and large changes.

RESULTS AND DISCUSSION

Surface Morphology

SEM micrographs of the untreated films reveal no surface texture or any other characteristic features. Figure 1 shows the surface morphology of the low draw ratio (1.6) PET films that have been solvent treated with DMF at various temperatures. Extensive surface cavitation and a spherulitic texture are visible, with the change from a smooth textureless surface to the cavitated morphology taking place almost instantaneously. The spherulite size for the films with a draw ratio of 1.6 is about 1–2 μm, which is in good agreement with measurements made by other workers.[4,5] The treatment temperature does not change the size of the spherulites appreciably, although the degree of cavitation increases with temperature. It appears that after treatment with DMF at 21°C the spherulites are covered by a layer or "matting" of polymeric material. Presumably, this layer consists of low-molecular-weight polymer that has been washed to the surface by the solvent. Nevertheless, the cavitation and the spherulites are visible. As the treatment temperature is increased, this matting is removed by dissolution in the DMF. The weight loss due to the DMF treatments reflects the removal of the surface matting. The weight loss for samples that have been DMF treated at 21°C is about 1%, while, after treatment at 145°C, the loss in weight can be as high as 9%.

In view of the weight loss, there is a possibility that the apparent cavitation reflects dissolution of the polymer from the surface as in an etching process. However, Makarewicz and Wilkes[5] have noted that cavitation also occurs in films that have been treated with DMF vapor where the possibility of material removal by dissolution is small. Furthermore, if a drop of DMF is placed on the film

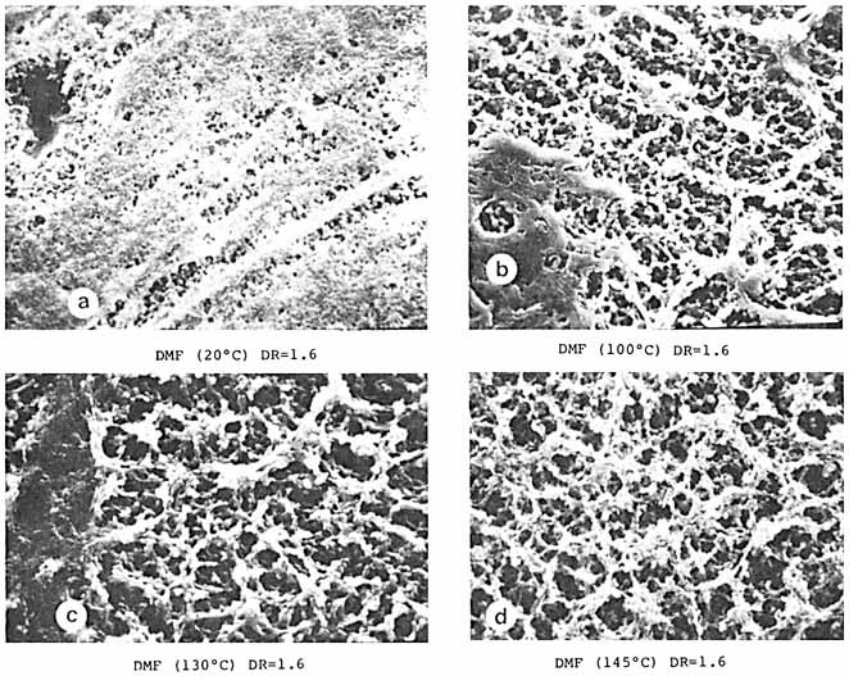

Fig. 1. Representative SEM's of the surface of DR 1.6 films treated in DMF at (a) 21°C, (b) 100°C, (c) 130°C, and (d) 145°C. The above films have been exposed to the 100°C water after rinse. 500×.

surface and then allowed to evaporate from that surface, the possibility of the solvent washing away the polymer from the surface is minimal. In such cases the cavitated structure and the spherulites are still clearly evident.

In order to reveal the depth of the spherulitic and cavitated layer, the treated films were subjected to cryogenic brittle fracture (liquid N_2), and the fracture surface analyzed by SEM. The results are shown in Figure 2. In the fracture surface of the untreated film, two zones are clearly visible. In the first (top) region the crack propagates along a smooth surface and after a certain point catastrophic failure takes place giving rise to a rough surface. The fracture surface of a film (DR 1.6) treated in DMF at 21°C shows that within the normally smooth top region the depth of the cavitated region is only about 15 μm. Three zones within that region are noticeable: (a) the highly cavitated outer surface, (b) a porous inner layer, and (c) a more tightly packed inner core.

With an increase in treatment temperature (DMF—145°C), the depth of the cavitated layer decreases, although the surface is cavitated to a greater extent. In the case of DMF treatments at 145°C, the films undergo both thermal and solvent crystallization with the former occurring more rapidly than the latter. The time scale over which the thermal crystallization occurs allows the solvent to penetrate only a small distance into the film, thereby restricting the cavitation depth. In this connection it should be noted that thermal annealing of DR 1.6 films at 145°C for 30 min completely stabilizes the structure by crystallization so that subsequent DMF treatment at 145°C induces no spherulitic structure and cavitation. As indicated in Paper I of this series, the intersection of the weight uptake curve with the ordinate at zero time may provide an estimate of the volume of the cavitated region.[1]

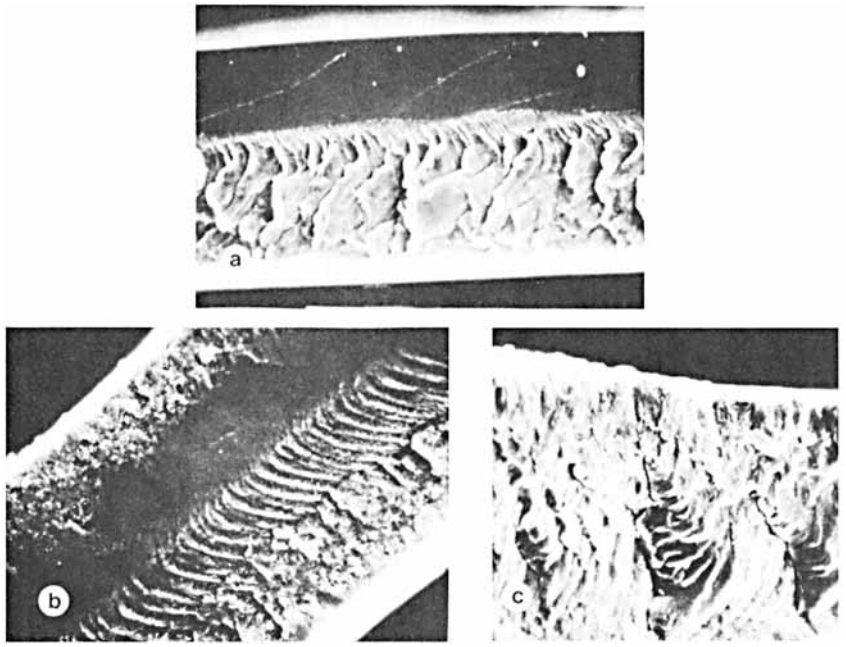

Fig. 2. Representative SEM's of the fracture surface of (a) DR 1.6 untreated, (b) DR 1.6 DMF (21°C), and (c) DR 1.6 DMF (145°C). 200×.

The effects of orientation (draw ratio) on the surface morphology resulting from DMF treatments at 145°C are summarized in Figure 3. Clearly, with in-

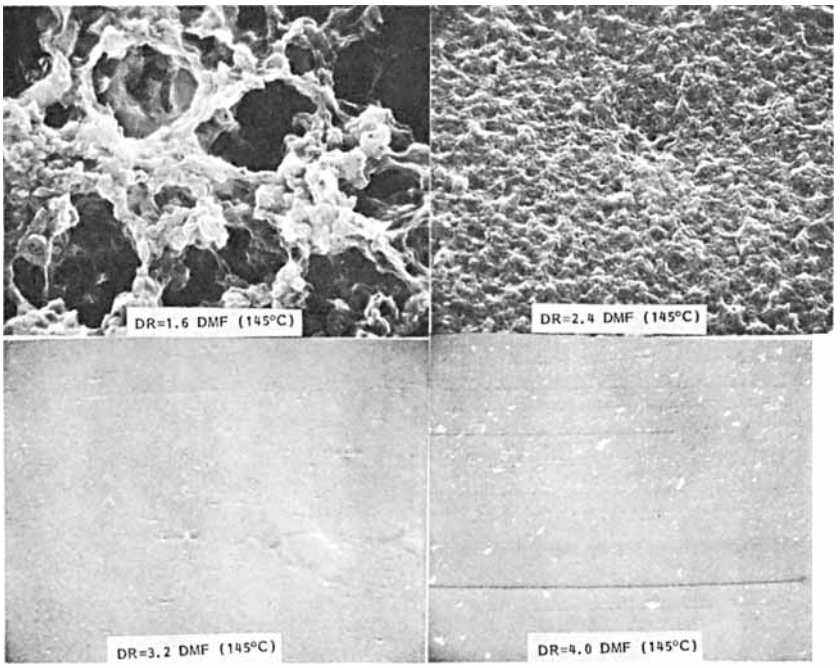

Fig. 3. Representative SEM's of the surface of (a) DR 1.6, (b) DR 2.4, (c) DR 3.2, and (d) DR 4.0 treated in DMF (145°C) followed by a 100°C water after rinse. 2,500×.

creasing orientation the DMF treatment causes less and eventually no observable modification in the surface texture. This reflects the stabilization of the film structure by the orientation and crystallization achieved during drawing. Treatments at lower temperatures are even less effective in causing surface cavitation of drawn films.

These studies indicate the wide range of surface morphologies that can be achieved with solvent crystallization by controlling preexisting orientation and crystallinity, treatment temperature, and thermal history. Undoubtedly variations in morphology can also be produced by use of different solvents.

Crystalline Structure

Wide angle x-ray scattering (WAXS) patterns of the untreated films of various draw ratios are shown in Figures 4 and 5. The photographs in Figure 4 are taken with the x-ray beam normal to the PET film surface (the draw direction is vertical). The patterns agree with the density data reported previously,[1] showing that a crystalline pattern begins to appear at DR 3.2. Below that level of drawing, even though the orientation increases, there is little crystallinity and only an amorphous halo is observable. At DR 4.0 the orientation and crystalline pattern is quite well developed, although amorphous scattering is present as a background. Figure 5 shows the diffraction patterns of the same films taken "edge

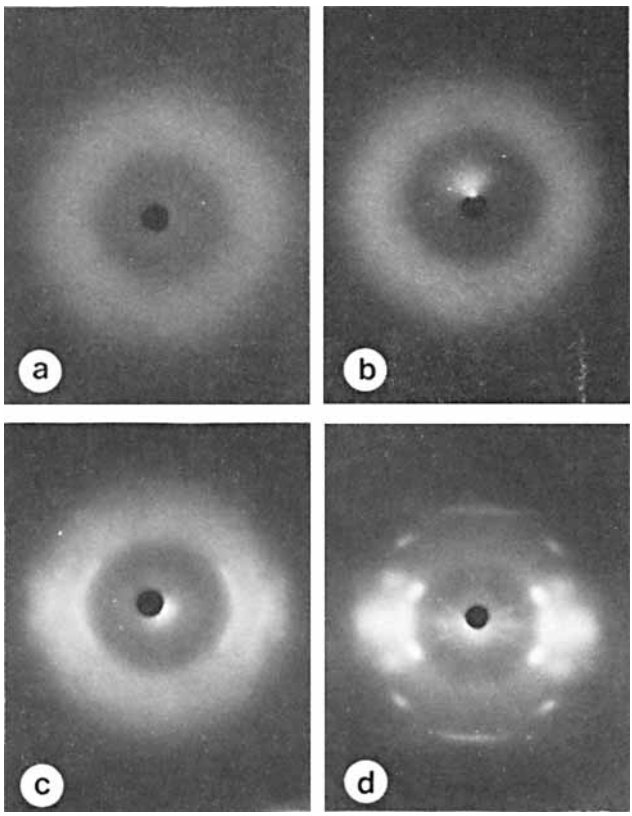

Fig. 4. WAXS patterns taken normal to the surface of untreated films of (a) DR 1.6, (b) DR 2.4, (c) DR 3.2, and (d) DR 4.0.

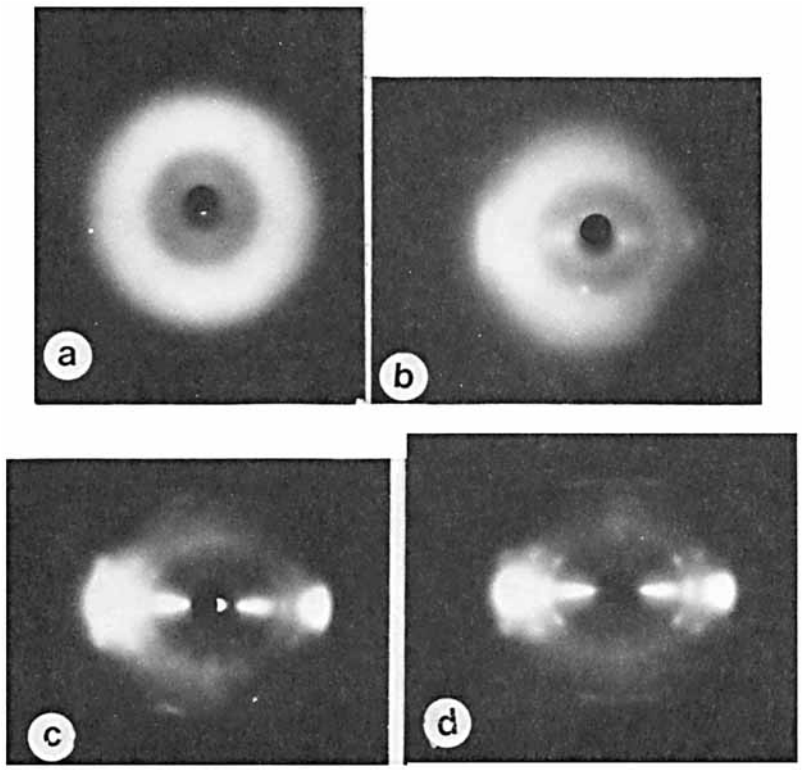

Fig. 5. WAXS patterns taken "edge on" of untreated films of (a) DR 1.6, (b) DR 3.2, (c) DR 3.6, and (d) DR 4.0.

on," with the draw direction vertical. The diffraction patterns in Figures 4 and 5 demonstrate that the PET films exhibit uniplanar orientation. With increasing draw ratio the benzene rings orient themselves more parallel to the surface as can be concluded from the intensity differences of the (010) and (100) diffraction arcs in Figures 4 and 5.

In Figures 6 and 7 are shown the WAXS patterns of films after thermal annealing at 145°C and after treatment in DMF at 145°C, respectively. In comparison to the WAXS patterns of the untreated films, it is clear that there is an increase in crystallinity for all draw ratios and a decrease in orientation for the films of higher draw ratios. The DMF treatments produce a better crystalline structure than the heat treatments, and the background and amorphous scattering is also lower in these films. After treatment with DMF at 145°C, the 010 and $0\bar{1}1$ peaks can be clearly distinguished even at the low draw ratios. Photographs shown in Figures 6, 7, and 8 are taken with the x-ray beam normal to the film surface.

In addition to information about crystallinity, the changes in crystallite orientation are also of interest. In the case of the highly drawn films, both the thermal (145°C) and the DMF (145°C) treatments cause considerable crystallite disorientation. Treatments at lower temperatures, for example at 21°C as shown in Figure 8, cause less disorientation but also a less well developed crystalline structure.

Calculated crystallite dimensions in the b direction were obtained from the

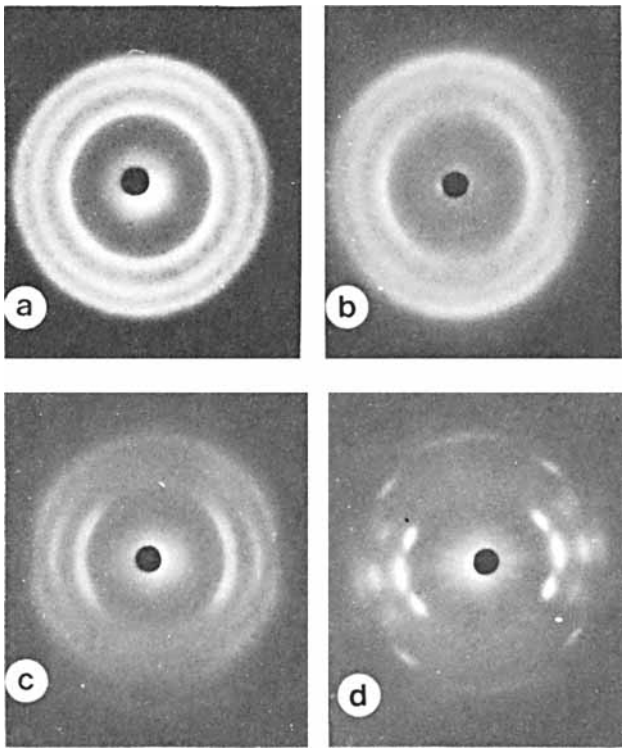

Fig. 6. WAXS patterns taken normal to the surface of heat (145°C) treated films of draw ratios (a) 1.6, (b) 2.4, (c) 3.2, and (d) 4.0.

(010) diffraction arc using the width at half-height technique,[32] and are plotted as a function of draw ratio in Figures 9 and 10 for various DMF and thermal treatments. In all the cases a maximum was found in the crystallite size at an intermediate draw ratio.

The crystallite size increases with an increase in the temperature of the DMF treatment, this being more prominent at the higher draw ratios, as shown in Figure 9. The 100°C water aftertreatment itself, following the treatment in DMF at 21°C, results in an improvement in the crystallite size. In the case of the DMF treatment at 21°C followed by water at 100°C for DR 3.6 and 4.0 films, the DMF itself induces little increase in crystallinity, and the only effect on structure is from the aftertreatment in water at 100°C (Fig. 10). For the lower draw ratio films there is a significant increase in crystallinity due to the DMF treatment, and there is little change as a result of the aftertreatment in water at 100°C.

Small Angle Scattering

Polymeric materials show two types of scattering at small angles—diffuse scattering which gives rise to a halo (Fig. 11) and discrete diffraction resulting in a ringlike scattering or streaks (Fig. 12). Diffuse scattering in solid polymers can be interpreted in terms of microvoids or intercrystalline space, and quantified in terms of the void size and the relative amount of void volume present. Discrete small angle diffraction provides information about the morphology of the system, the "long spacing" providing data about the crystalline and intercrystalline thicknesses (their sum), and about their uniformity and shape.

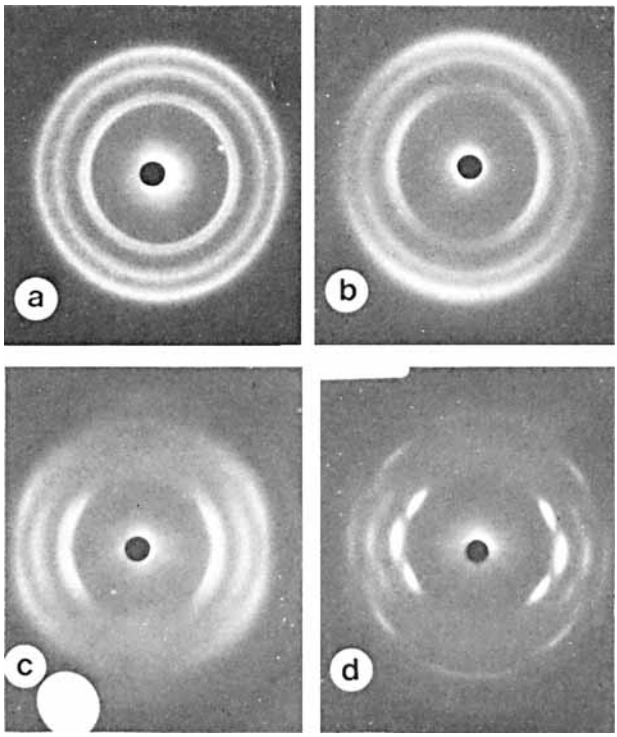

Fig. 7. WAXS patterns taken normal to the surface of DMF (145°C) + H_2O (100°C) treated films of draw ratios (a) 1.6, (b) 2.4, (c) 3.2, and (d) 4.0.

Calculated values of long period spacings are shown in Table I. Since many of the films treated in DMF exhibit an intense diffuse scattering which masks the discrete scattering, long spacings could be measured only for samples where the void scattering was absent or minimal. For the untreated films discrete scattering was visible only for films of DR 4.0 corresponding to a long spacing of 120 Å. After 145°C thermal treatments, the calculated long period spacings are approximately equal for the different draw ratios. Although the spacings are similar, the shape of the patterns differ, as shown in Figure 12. At the lowest draw ratio, a ring scattering corresponding to a spherically symmetrical collection of crystallites as in a spherulite is found. With increasing draw, the discrete scattering corresponds to stacked lamellar crystals which have a distribution of orientations about the stretch axis. At DR 4.0, meridional streaks are visible, indicating that the lamellar or fibrillar surfaces of the crystallites are arranged perpendicular to the orientation direction. (As in most of the WAXS photographs, the x-ray beam in the SAXS pictures is normal to the PET film surface. Usually in such patterns of PET films, the scattering patterns taken normal to the surface and "edge on" are different. The streaks may be continuous or resolved into four streak patterns depending on the orientation of the intercrystalline areas with respect to the draw direction.[33] The lateral width of the lamellae also increased due to the heat treatment, as can be deduced from the horizontal breadth of the pattern.[33,34]

Other treatments for which discrete scattering was visible are shown in Table I. The long period can be measured for the higher draw ratios even after the

TABLE I
Long Period Spacing

DR	Treatment	Long spacing (Å)
4.0	untreated	120
1.6	heat (145°C)	120
2.4		115
3.2		112
4.0		118
1.0	DMF (21°C)	73
1.6		70
2.0		73
2.4		74
2.8		78
3.2		93
4.0		120
3.6	DMF (145°C)	140
4.0		138

severe (145°C) DMF treatments, since the diffuse scattering is not intense. The DMF treatments at 21°C induce a structure where the spacing is much smaller, except at the highest draw ratio, where the spacing corresponds to that of the original untreated material.

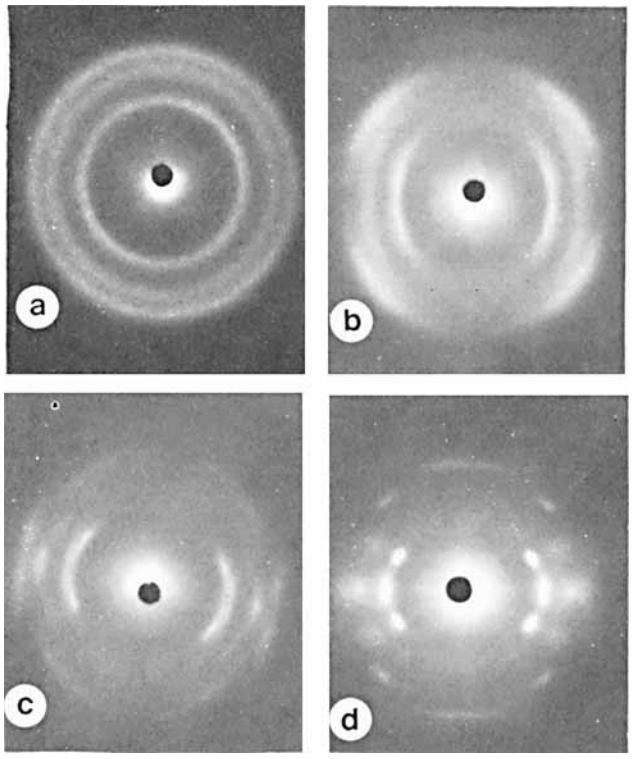

Fig. 8. WAXS patterns taken normal to the surface of DMF (21°C) + H_2O (100°C) treated films of draw ratios (a) 1.6, (b) 2.4, (c) 3.2, and (d) 4.0.

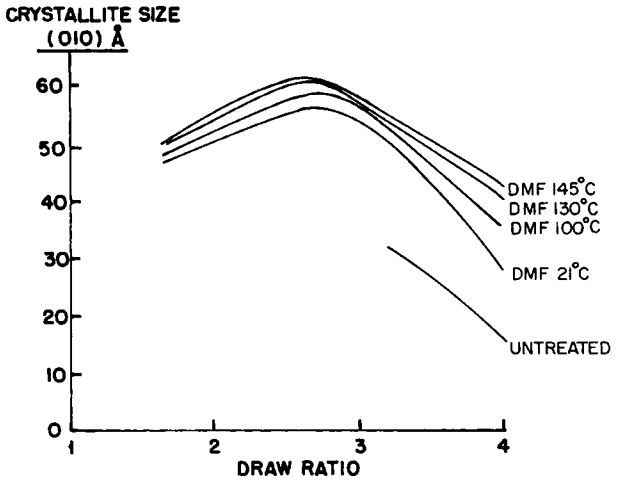

Fig. 9. Crystallite size (010) as a function of the draw ratio for various DMF treatment temperatures.

Examples of diffuse or void scattering are shown in Figure 11. From microdensitometer scans of the patterns, plots of small-angle intensity times the angle as a function of the angle were constructed and extrapolated to angles limited by the beam stop. In all cases the curves start to converge towards the origin after passing through a maximum. This method limited the error caused by the extrapolation since it eliminated the possibility of errors due to the extreme steepness of the intensity curve near the origin. In Figure 13 are shown such plots for films of different draw ratios that have been treated in DMF at 145°C. The void content is the highest for the solvent crystallized DR 1.6 film and decreases with increasing draw ratio. Presumably the voids form due to crystallization taking place while the polymer is in a swollen state. At low draw ratio, the swelling is quite significant and a greater void volume results than in DR 4.0 where the existing crystalline structure limits both the extent of swelling and the change in crystallinity.

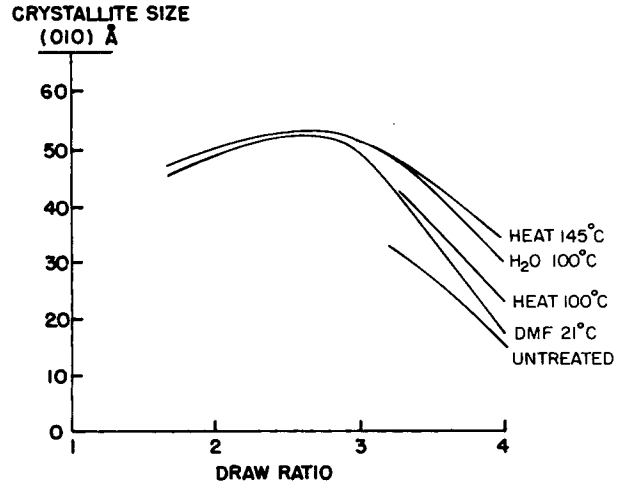

Fig. 10. Crystallite size (010) as a function of the draw ratio for various heat and DMF treatments.

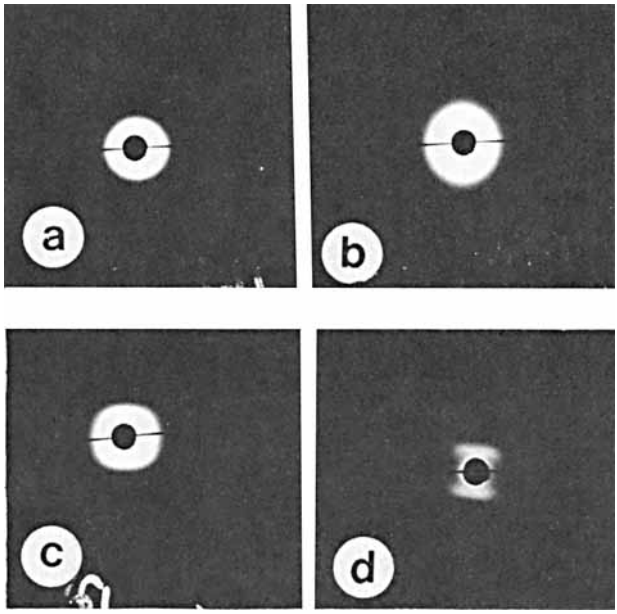

Fig. 11. SAXS patterns of DMF (145°) + H_2O (100°C) films of draw ratios (a) 1.6 exposed for 2 h, (b) 2.4 exposed for 6 h, (c) 3.2 exposed for 12 h, and (d) 4.0 exposed for 10 h.

Treatment temperature and the mode of DMF removal also have an effect on the void volume. The effect of temperature is illustrated in Figure 14. Treatment at 145°C induces a greater void volume in the 1.6 draw ratio film than

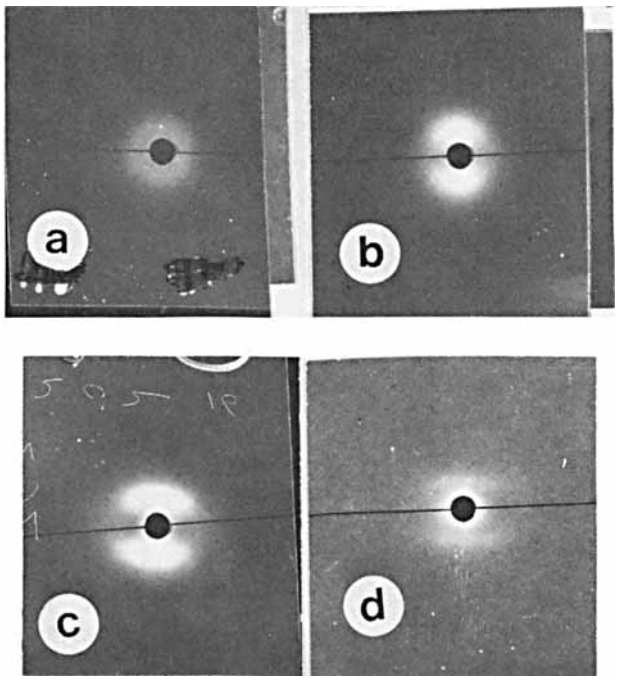

Fig. 12. SAXS patterns of heat (145°C) treated films of draw ratios (a) 1.6 exposed for 4 h, (b) 2.4 exposed for 8 h, (c) 3.2 exposed for 16 h, and (d) 4.0 exposed for 30 h.

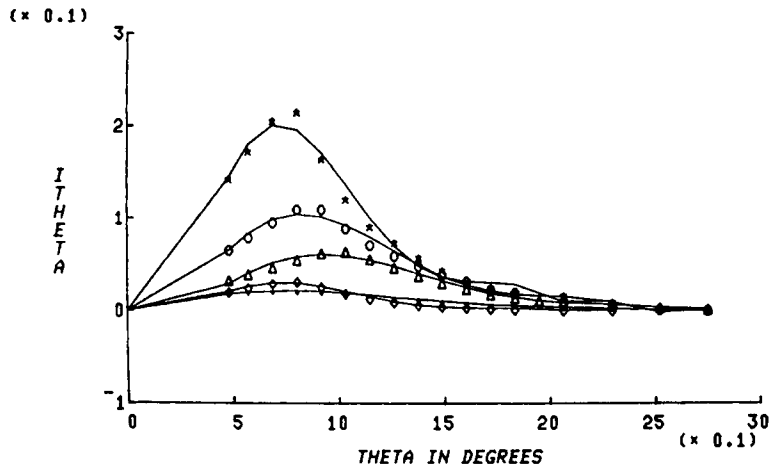

Fig. 13. Small angle intensity times the angle vs. the angle in degrees for DMF (145°C) + H_2O (100°C) treated films of various draw ratio: (*) 1.6; (○) 2.9; (△) 2.4; (◇) 3.2; (●) 3.6.

treatment at 21°C. Weigmann[11–14] had previously found that very little diffuse scattering was visible in oriented yarns after DMF treatments at temperatures below 120°C. In oriented films void scattering is discernible only after the high temperature treatment. It is only at these high temperatures that any significant swelling can take place together with the partial melting and crystallization of the existing crystalline structure. Both the above conditions are necessary for void formation.

The mode of DMF removal also affects the void structure, as illustrated in Figure 15. The largest void fraction results if the DMF is removed using the 100°C water aftertreatment. Removal of DMF by slow air drying at room temperature gives a lower void volume after most of the DMF has been eliminated. Removal of DMF by air drying at an elevated temperature (100°C) causes the collapse of the voids due to the pasticizing action of the DMF. In water at 100°C, even though the temperature is the same, there is little or no collapse of

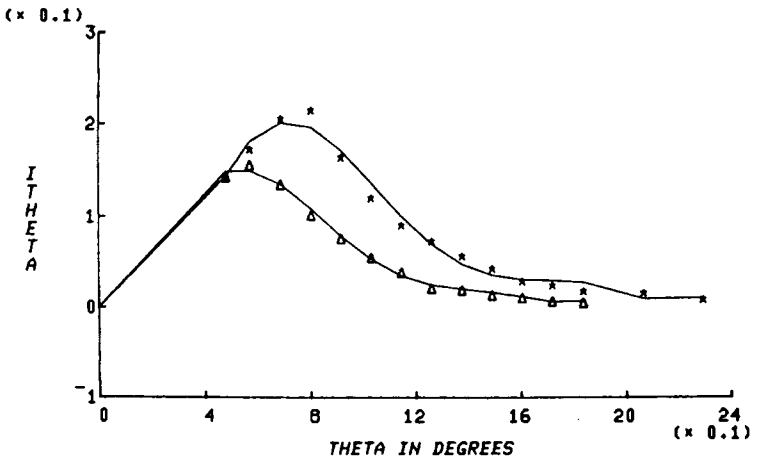

Fig. 14. Small angle intensity times the angle vs. the angle for DMF (21°C) + H_2O (100°C) (△) and DMF (145°C) + H_2O (100°C) (*) treated films of draw ratio 1.6.

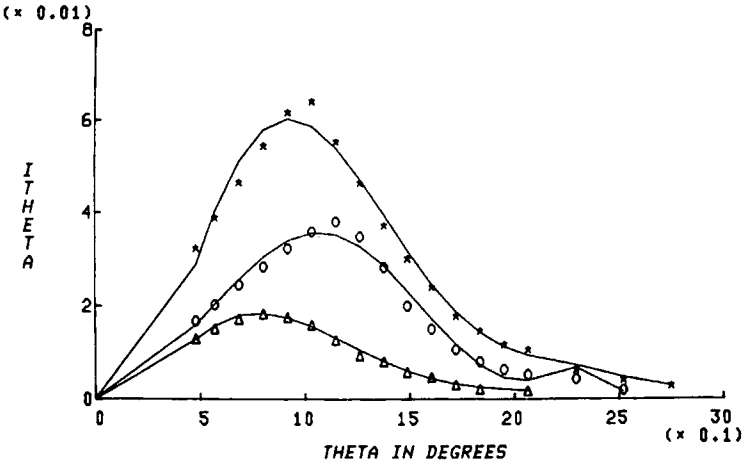

Fig. 15. Small angle intensity times the angle vs. angle in degrees for various methods of DMF removal: (*) 2.4 DMF (145°C) + H_2O (100°C); (○) 2.4 DMF (145°C); (△) 2.4 DMF (145°C) + HT (100°C).

the void structure since removal of the DMF takes place by water displacement. Obviously, the thermal stability of the voids is also of interest, and the decrease in the void scattering with various heat aftertreatments is shown in Figure 16. As the severity of the thermal aftertreatment is increased, the total void volume decreases, probably reflecting the collapse of some of the crystallites which stabilize the void structure.

Attempts to measure the void size, revealed no systematic differences. The void size is much the same for all cases and only their concentration differs with the treatment conditions. Using Guinier plots the voids appear to have a radius of gyration of approximately 20 Å corresponding to a void radius of about 25.8 Å.

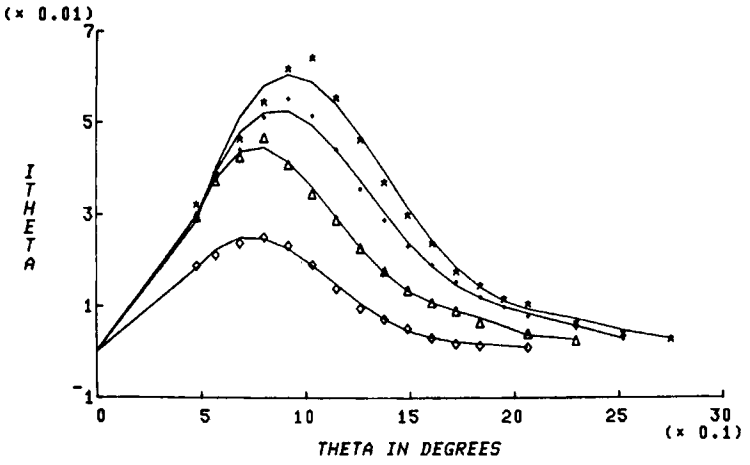

Fig. 16. Small angle intensity times the angle vs. angle in degrees for draw ratio 2.4 films treated in DMF (145°C) + H_2O (100°C) followed by various heat aftertreatments: (*) —; (●) 100°C; (△) 150°C; (◇) 200°C.

Differential Scanning Calorimetry

Three peaks can be observed in DSC scans of the untreated films as shown in Figure 17, reflecting the following events: the glass transition, crystallization, and melting. The glass transition temperatures of the untreated PET films are shown in Table II for the various draw ratios. There is no significant change in the T_g with draw ratio as measured on the DSC, although T_g as measured from the dynamic elastic modulus (E') using the Rheovibron® increases with increasing orientation.[1] The T_g of the films is clearly visible only to a DR 3.2, after which only a minor deflection is observed.

It has been shown that the thermal history of polyester can be established from DSC melting behavior.[26] When a sample of PET has been subjected to a sufficiently high heat treatment, a small endotherm characteristic of the thermal treatment is noticeable in the melting behavior as a double melting peak. The first peak has been referred to as the premelting endotherm (T_m). DSC fusion curves, recorded at high instrument sensitivity for the samples that have been

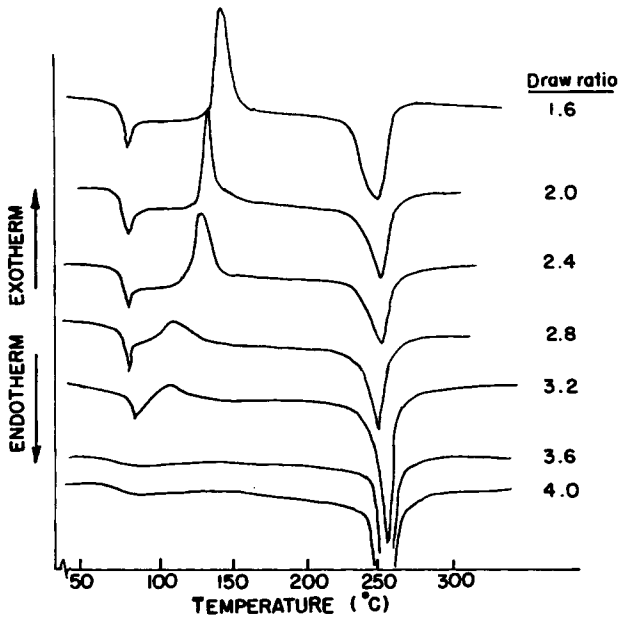

Fig. 17 DSC scans of the untreated PET films of various draw ratios.

TABLE II
Transition Temperatures of Untreated Films

DR	T_g (°C)	T_c (°C)	T_m (°C)	T_g, Rheovibron (°C)
1.6	82	144	251	97
2.0	82	135	251	105
2.4	81	130	251	
2.8	82	112	252	110
3.2	83	105	255	120
3.6			256	131
4.0			256	144

heat treated at 145°C, are shown in Figure 18 with the premelting endotherm visible between 150°C and 155°C, before the main melting peak (off scale). The behavior of the drawn and undrawn samples is quite similar with respect to the position of the premelting endotherm.

DSC thermograms after DMF treatments at various temperatures are shown in Figures 19–22. After DMF treatments at 21°C a broad peak is visible at

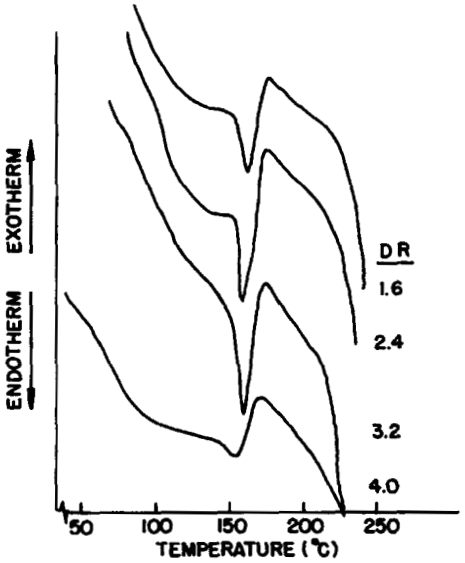

Fig. 18. Premelting DSC curves of heat (145°C) treated PET films of draw ratios 1.6, 2.4, 3.2, and 4.0.

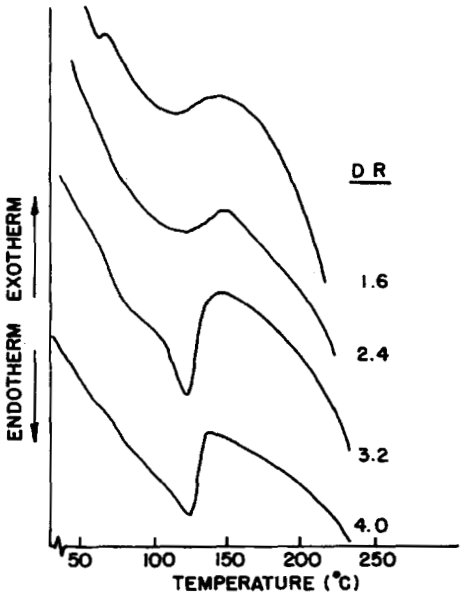

Fig. 19. Premelting DSC curves of DMF (21°C) + H_2O (100°C) treated films of draw ratios 1.6, 2.4, 3.2, and 4.0.

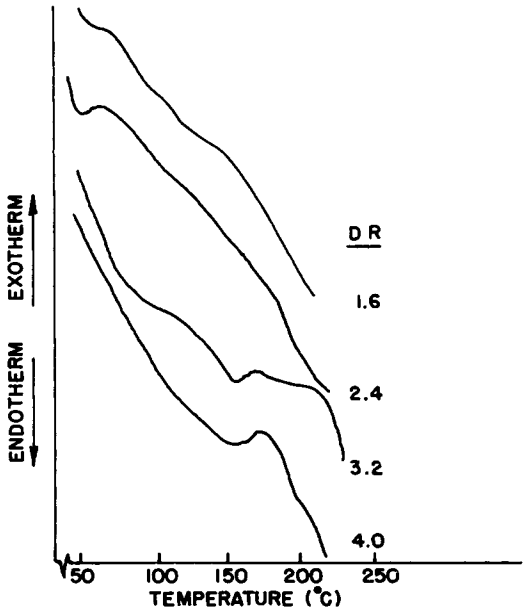

Fig. 20. Premelting DSC curves of DMF (100°C) + H_2O (100°C) treated films of draw ratios 1.6, 2.4, 3.2, and 4.0.

120–125°C, which can be associated with the 100°C water aftertreatments to which the films are subjected after the solvent crystallization. If this water treatment is omitted, no premelting endotherm is visible. DMF treatments at 100°C show a small premelting endotherm for films with draw ratios of 3.2 and 4.0 at about 165°C (Fig. 20). Crystallites formed at DR 1.6 and DR 2.4 have a

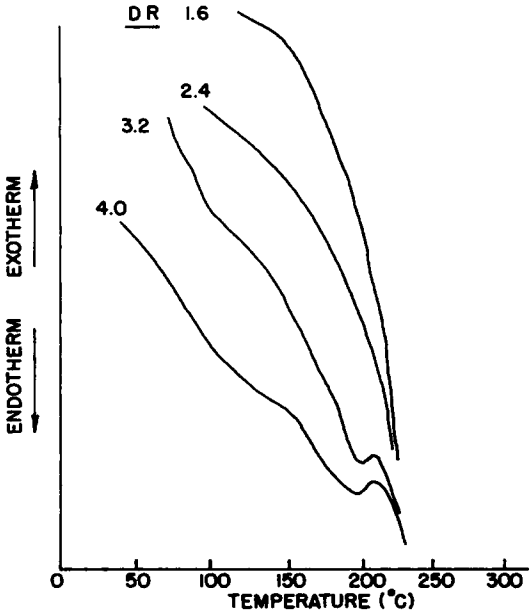

Fig. 21. Premelting DSC curves of DMF (130°C) + H_2O (100°C) treated films of draw ratio 1.6, 2.4, 3.2, and 4.0.

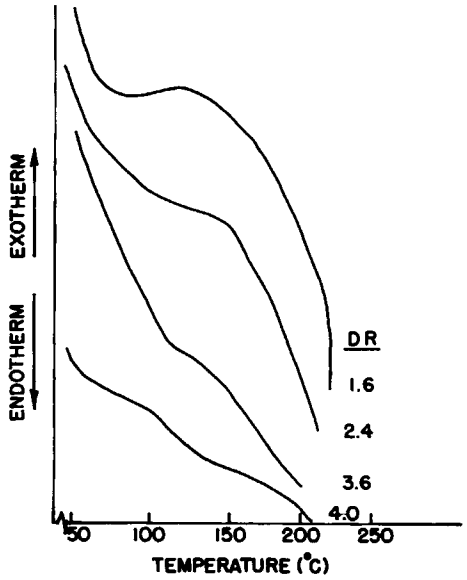

Fig. 22. Premelting DSC curves of DMF (145°C) + H_2O (100°C) treated films of draw ratio 1.6, 2.4, 3.2, and 4.0.

perfection that is not characteristic of any temperature and the entire sample melts within the main melting event (off scale).

The same features are also observable in the melting behavior of films treated in DMF at 130°C (Fig. 21). At DR 3.2 and DR 4.0 the premelting endotherm appears at about 197°C. The lower draw ratios of 1.6 and 2.4 again do not show a premelting endotherm. As the treatment temperature is increased to 145°C, no premelting endotherm is observable over the whole range of draw ratios (Fig. 22). The characteristic crystallites that exist at the higher draw ratios melt with the bulk and only the main melting peak is observed.

The authors are pleased to acknowledge many helpful discussions with Dr. H.-D. Weigmann of TRI. The work was made possible by grants from the National Science Foundation (Grant No. 76-80570) and from the Camille and Henry Dreyfus Foundation.

References

1. H. Jameel, J. Waldman, and L. Rebenfeld, *J. Appl. Polym. Sci.*, **26**, 1795 (1981).
2. R. G. Quynn, M. A. Sieminski, and J. L. Riley, *J. Text. Inst.*, **55**(11), T566 (1964).
3. L. Cottam, R. P. Sheldon, D. A. Hemsley, and R. P. Palmer, *Polym. Lett.* **2**, 761 (1964).
4. A. B. Desai and G. L. Wilkes, *J. Polym. Sci. Sympos. No. 46*, 291 (1974).
5. P. J. Makarewicz and G. L. Wilkes, *J. Polym. Sci.*, **16**, 1529 (1978).
6. B. H. Knox, H.-D. Weigmann, and M. G. Scott, *Text. Res. J.*, **45**, 203 (1975).
7. A. S. Ribnick, H.-D. Weigmann, and L. Rebenfeld, *Text. Res. J.*, **43**, 176 (1973).
8. A. S. Ribnick and H.-D. Weigmann, *Text. Res. J.*, **43**, 316 (1973).
9. H.-D. Weigmann and A. S. Ribnick, *Text. Res. J.*, **44**, 176 (1974).
10. H.-D. Weigmann and M. G. Scott, *Text. Res. J.*, **45**, 554 (1975).
11. H.-D. Weigmann, M. G. Scott, A. S. Ribnick, and L. Rebenfeld, *Text. Res. J.*, **46**, 574 (1976).
12. H.-D. Weigmann, M. G. Scott, A. S. Ribnick, and R. D. Matkowsky, *Text. Res. J.*, **47**, 745 (1977).
13. H.-D. Weigmann, M. G. Scott, and A. S. Ribnick, *Text. Res. J.*, **47**, 761 (1977).
14. H.-D. Weigmann, M. G. Scott, and A. S. Ribnick, *Text. Res. J.*, **48**, 4 (1978).
15. H. Zachmann, *Faserforsch. Textiltech*, **18**, 95 (1967).

16. H. Zachmann, *Makromol. Chem.*, **74,** 29 (1964).
17. V. Eichoff and H. Zachmann, *Makromol. Chem.*, **147,** 41 (1971).
18. H. Zachmann and W. Schermann, *Kolloid Z. Z. Polym.*, **241,** 916 (1970).
19. E. L. Lawton and D. M. Cates, *J. Appl. Polym. Sci.*, **13,** 899 (1969).
20. P. J. Makarewicz and G. L. Wilkes, *J. Appl. Polym. Sci.*, **22,** 3347 (1978).
21. L. Cottam and R. P. Sheldon, *Adv. Polym. Sci. Technol.*, **26,** 65 (1966).
22. E. Gerold, L. Rebenfeld, M. G. Scott, and H.-D. Weigmann, *Text. Res. J.*, **49,** 652 (1979).
23. M. Ikeda, *Chem. High Polym.* Jpn., **25**(273), 87 (1968).
24. R. C. Roberts, *Polym. Lett.*, **8,** 381 (1970).
25. P. J. Holdsworth and A. Turner-Jones, *Polymer*, **12,** 195 (1971).
26. G. Hiedeman and H. J. Bendt, *Chem.* Text. **24/76,** 46 (1974).
27. J. P. Bell and T. Murayama, *J. Polym. Sci.* (*A-2*), **7,** 1059 (1969).
28. R. C. Roberts, *Polymer*, **10,** 117 (1969).
29. R. P. Sheldon, *Polymer*, **4,** 213 (1963).
30. P. J. Makarewicz and G. L. Wilkes, *Text. Res. J.*, **48,** 136 (1978).
31. G. C. Adams, *Polym. Eng. Sci.*, **19,** (6) 456 (1979).
32. H. P. Klug and L. E. Alexander *X-ray Diffraction Procedures for Polycrystalline and Amorphous Materials*, 2nd ed., Wiley-Interscience, New York, 1974, Chap. 9.
33. W. O. Statton and G. M. Goddard, *J. Appl. Phys.*, **28,** 1111 (1957).
34. E. A. Bolduan and R. S. Bear, *J. Polym. Sci.*, **6**(3), 271 (1951).

Received May 14, 1981
Accepted August 13, 1981